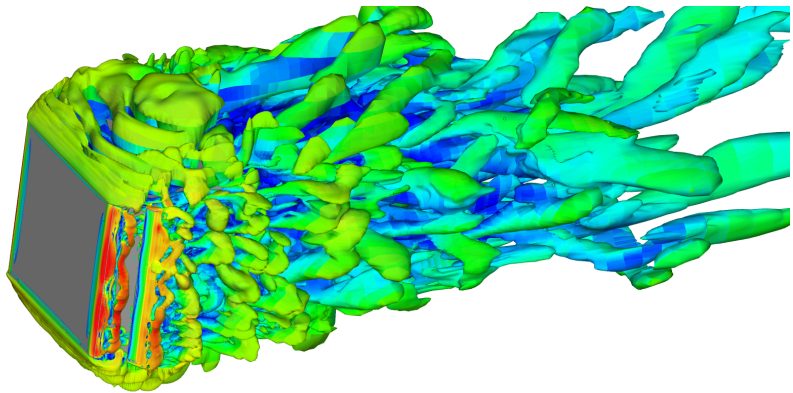


CHALMERS



Active Flow Control for Reduction of Aerodynamic Drag on a Simplified Truck Model with side mirror

Investigation of the effects of a synthetic jet actuator

Master's thesis in Computational Fluid Dynamics

VIJAIKRISHNA TATCHANAMOORTHY

Department of Applied Mechanics

Division of Fluid Dynamics

CHALMERS UNIVERSITY OF TECHNOLOGY

Göteborg, Sweden 2017

Master's thesis 2017:75

MASTER'S THESIS IN COMPUTATIONAL FLUID DYNAMICS

Active Flow Control for Reduction of Aerodynamic Drag
on a Simplified Truck Model with side mirror

Investigation of the effects of a synthetic jet actuator

VIJAIKRISHNA TATCHANAMOORTHY

Department of Applied Mechanics
Division of Fluid Dynamics
CHALMERS UNIVERSITY OF TECHNOLOGY
Göteborg, Sweden 2017

Active Flow Control for Reduction of Aerodynamic Drag on a Simplified Truck Model
with side mirror
Investigation of the effects of a synthetic jet actuator
VIJAIKRISHNA TATCHANAMOORTHY

© VIJAIKRISHNA TATCHANAMOORTHY, 2017

Master's thesis 2017:75
Department of Applied Mechanics
Division of Fluid Dynamics
Chalmers University of Technology
SE-412 96 Göteborg
Sweden
Telephone: +46 (0)31-772 1000

Chalmers Reproservice
Göteborg, Sweden 2017

Acknowledgement

I would like to express my gratitude to my thesis supervisor Prof. Sinisa Krajinovic, for being patient and encouraging me to complete my thesis. I would also like to express my gratitude to colleagues, Srikanth, Abhishek Saraf, raj Kiran and Aniruth Rao for their help during my masters studies and thesis. Thankful to Aniruth Rao and Guglimo Minelli for providing their valuable resources and time on my thesis. Special thanks to Abhishek Saraf for improvising and giving reviews about my thesis report. Finally, I would like to express my gratitude towards my parents.

Abstract

These days consumption of fuel plays the major role in automotive industry. Major plans are made to reduce fuel consumption and to cut the cost and emissions of the vehicle there should be reduction in the drag force. Recently based on research, use of Active Flow Control (AFC) has reduced the drag force. In this thesis AFC is introduced in the form of synthetic jet actuator at the A-pillar of the simplified truck along with the side mirrors and the amount of reduction in drag will be discussed in detail. In this thesis majorly 2 simulations are carried out one with the normal reference case without actuation of AFC and compared with the one with the case with actuation of AFC at the frequency, amplitude values are based on the research paper [1]. The unsteady turbulent simulations are carried out using the Partially-Averaged Navier-Stokes (PANS) turbulence model.

Nomenclature

Symbols

F_D	Drag force	N
C_D	Drag coefficient	
A	Frontal area	m^2
U_∞	Free-Stream velocity	m/s
Δ	Cell Grid Dimension	m
L	Length Scale	m
T	Time Scale	s
Δt	Time step	s
Δx	Cell length	m
U_i	Average velocity	m/s
Λ	Turbulence length scale	m
V_i	Instantaneous velocities	m/s
k	Turbulent kinetic energy	m^2/s^2
ε	Turbulent dissipation	m^2/s^3
τ_w	Wall shear stress	Pa
ζ	Velocity scale ratio	
$C_1 C_2$	Model constants	
$F_{D,friction}$	Skin frictional force	N
ρ_∞	Free stream density	kg/m^3
τ	Subfilter scale stress	m^2/s^2
ν_t	Turbulent viscosity	m^2/s
ν	Eddy viscosity	m^2/s
S_{ij}	Resolved stress tensor	$1/s$
u^*	Friction velocity	m/s
I	Turbulent intensity	
f	Frequency	Hz
y^+	Dimensionless wall distance	
$F_{D,pressure}$	Pressure drag force	N

Subscripts

A	of the AFC
r	resolved quantity
u	unresolved quantity

Acronyms

CFD	Computational Fluid Dynamics
AFC	Active Flow Control
ZNMF	Zero Net Mass Flux
PANS	Partially Averaged Navier-Stokes
LES	Large Eddy Simulation
RANS	Reynolds Averaged Navier-Stokes
URANS	Unsteady Reynolds Averaged Navier-Stokes
DDES	Delayed Detached Eddy Navies Stokes

CONTENTS

Contents

1	Introduction	1
2	Theory	1
2.1	Drag coefficient C_D	2
2.2	Active Flow Control	2
2.3	Introduction to Governing equation and Turbulence	3
2.3.1	Governing equations	3
2.3.2	continuity equations	3
2.3.3	The Momentum equations	4
2.3.4	Selection of Turbulence model	4
2.3.5	Partially Averaged Navier-Stokes	5
3	Model Description	7
3.1	Geometry	7
3.2	Blocking and Meshing	9
3.2.1	Blocking	9
3.2.2	Meshing	10
3.3	Numerical set-up	12
3.4	Post-processing	13
4	Results and discussion	14
4.1	Un-actuated flow	14
4.2	comparison between controlled and uncontrolled flow	17
5	Conclusions and future work	22
	References	24

1 Introduction

Heavy vehicle fuel consumption plays a vital role in high transport costs and increase in global temperatures due to emissions, thereby increasing the demand for fuel efficient vehicles. The Heavy commercial vehicles have an un-streamlined body shape due to various restrictions like length, height, width of the vehicle which in-turn are considered as aerodynamically inefficient. A truck moving at a speed of “100 Km/hr” consumes approximately 52 percent of overall fuel to overcome the aerodynamic drag. This made researchers to concentrate on the aerodynamics of heavy vehicles and to find the solution and methods to reduce the aerodynamic drag significantly. There are basically two types to reduce aerodynamic drag either by passive or Active flow control methods. Passive control techniques like platooning, trailer add-on, camera mirrors are used to reduce drag.

Cameras are used instead of side mirrors to reduce the frontal area of the truck which in turn leads to drag reduction, still side mirrors are preferred by the drivers to act as fail-proof device in case of camera failure and severe climatic conditions. So truck manufactures include the side mirrors. In this study the flow around the truck was controlled by Active Flow Control (AFC). AFC has some advantages which act in a closed-loop i.e., it gives feedback for the better control over flow. AFC can also be used for aerodynamic purposes to reduce the flow separation. Among the various AFC techniques, a Zero Net Mass Flux (ZNMF) is selected for its wide operating frequencies. This study was designed to discuss the aerodynamic effects of side mirrors on simplified geometry truck where Active Flow Control is introduced at the A-Pillar of the truck.

Among various turbulence models Partially Averaged Navier-Stokes (PANS) was selected since Large Eddy Simulation (LES) needs large computational time and also reduces accuracy for the detailed bluff bodies. PANS model has proven to give more accurate results for the bluff body flows [1]. This work is the continuation of previous paper [1]. Previous work has determined an optimal frequency and actuation velocity for the AFC to reduce the separation of flow along the A-pillar of the truck. The next step was towards the implementation in a simplified truck with side mirrors which was pursued in this study, in which the flow patterns were investigated and the effect of side mirrors for the aerodynamic drag was studied.

2 Theory

This section gives basic knowledge to the concepts used to solve most of the aerodynamic problem. This chapter can be divided into two divisions. one by explaining intricate concept of Drag coefficient C_D , active flow control and other gives the basic introduction to the turbulence models and promotes the need for the PANS

turbulence model.

2.1 Drag coefficient C_D

In aerodynamics, drag force could be major issue for the vehicles. Drag force is imagined in two perspectives, through the vehicle and through the surrounding fluid. From the vehicle's perspective, it is the pressure and the friction components involved in the physics. The most significant is majorly the pressure drag for road vehicles, and friction drag for air-crafts and ships. Design of vehicle aerodynamics could influence the drag force reduction of drag force implements several benefits, namely the increased capability of acceleration, increased top speed, and reduction in fuel consumption.

So, drag force is addition of both pressure force and skin friction force

$$F_D = F_{D,s} + F_{D,p} \quad (2.1)$$

From the fluid flow perspective, it is important to discuss about the consequences of drag. As a result of drag, wakes are formed in different portions of the vehicle. dimensionless drag coefficient is useful to represent the characteristic drag.[2]

$$C_D = \frac{F_D}{\frac{1}{2}\rho_\infty AU_\infty^2} \quad (2.2)$$

2.2 Active Flow Control

Active flow control requires actuators to function as flow disturbance device. Actuators can also behave as sensors when there are ideal. This advantage of actuators is used to get the better information of flow and frequency of the flow structures, accordingly actuation can be varied for flow field requirements. Recent researches [3] provide information that actuators also be used as flow manipulation device to reduce the aerodynamic losses.

There are many type of actuators and they can be divided into four types: plasma, moving object/surface, fluidic and other(e.g, electromagnetic, magneto-hydrodynamic)[3]. Among all these types fluidic or synthetic jet actuators considered to be the most effective since, it does not require fluid injection, wide range of frequency operation, high performance and feedback control. Synthetic jet actuator or Zero Net Mass Flux (ZNMF) has a piezoelectric diaphragm which oscillates at its equilibrium state there by providing the change in the cavity volume which alternatively blow and suck the fluid from orifice.

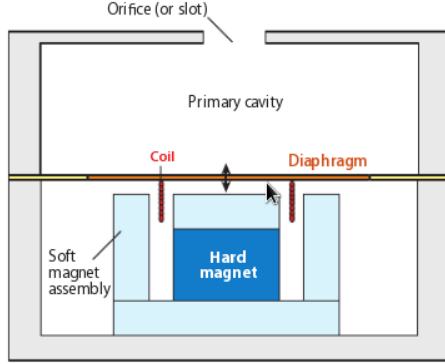


Figure 2.1: *Schematic of a synthetic jet actuator [3]*

2.3 Introduction to Governing equation and Turbulence

This section provides basic knowledge about transport equations to solve fluid flow problem in given computational domain.

The basic equation for solving fluid flow problem are Navier-stokes equation, these equations require very fine mesh and consumes more time to solve large Reynolds flow problems so, there are various closure models to solve fluid flow problem each has their own advantages and disadvantages.

2.3.1 Governing equations

2.3.2 continuity equations

Balance of mass equation is the basic continuity equation which reads.

$$\frac{\partial \rho}{\partial t} + \rho \frac{\partial v_i}{\partial x_i} = 0. \quad (2.3)$$

When the flow is in-compressible ($\rho = \text{const}$) equation becomes,

$$\frac{\partial v_i}{\partial x_i} = 0. \quad (2.4)$$

2.3.3 The Momentum equations

The momentum equation is formulated from constitutive law in newtonian viscous fluid.

$$\rho \frac{\partial v_i}{\partial t} + \rho \frac{\partial v_i \partial v_j}{\partial x_j} = - \frac{\partial P}{\partial x_i} + \mu \frac{\partial^2 v_i}{\partial x_j \partial x_j} \quad (2.5)$$

Eq. 2.4 and Eq. 2.5 are the Navier-stroke equation.

2.3.4 Selection of Turbulence model

The transport equations in fluid mechanics are arrived from the Navier-Stokes equations. Resolving the instantaneous velocities at high Re is very difficult due to requirement of large computational resources. It is not possible to predict the unsteady flow around the bluff bodies using RANS, since the the eddies of all sizes in the flow are scaled in to one turbulent scale. However, due to the absence of large eddies near the walls, it is feasible to use RANS near the walls. Direct numerical simulation (DNS) resolves the entire turbulent scales in the energy spectrum but at low Re . Moreover DNS requires a fine computational grid in resolving the flow which is time consuming and expensive.

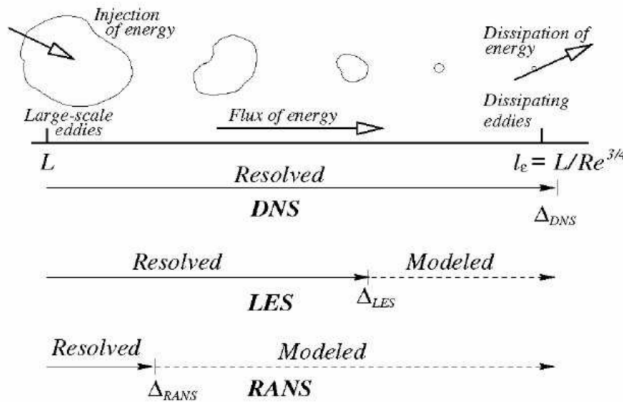


Figure 2.2: Representation of modelling scale [4]

The way to make the RANS take fluctuations into account is to make unsteady, which is done by adding an unstable term to the equations. But that didn't improve

the accuracy very much, especially in a flow with separation.

So the DES(Detached Eddy simulation) invented in order to overcome the poor predictability of URANS in the wake region and reduce the larger computational power needed by LES in the boundary layer flow.

There are many turbulence models were proposed, the LES model could predict the fluid flow for low Reynolds number flow. LES cannot be used for the industrial analysis, since they use high reynolds number to calculate the fluid flow. LES is not the best option for high reynolds number flow. Especially for the fluid having the sharp eddy separation could require the fine computational grids. The RANS model is proposed in order to calculate the flows having the high reynolds number, but this model is steady flow model. Then URANS model is proposed by making RANS model into unsteady by adding unsteady term in the transport equation. This model doesn't seem to hold good for the flow separation flows. So the DES (Detached Eddy simulation) is found in order to overcome the poor predictability of URANS in the wake region by calculating wake portion using LES.

From [5], a conclusion could be made that the DES model predicts the flow separation well but when the yaw angle is increased, this model shows the mismatch of pressure close to the base, when compared with the experimental data, so DES approach still has the modelling error and discretization error.

Then DDES(Delayed Detached Eddy Simulation) model is proposed to minimise the error produced by the DES model, but both the models suffer the miss match between the modelled log layer and resolved log layer[6]. Later PANS model is proposed [7] which seems to capture the flow separation better when compared with other models with less time consumption. The Partially Averaged Navier-Stokes is a hybrid RANS-DNS turbulence model. The detailed explanation of PANS method as follows in next section.

2.3.5 Partially Averaged Navier-Stokes

The PANS uses the bridging technique called variable resolution, so this method acts as a RANS or DNS based on clouse technigue. This method is proposed by Han et al.[8] read

$V_i = U_i + u_i$ where U_i is resolved velocity or *filtered* velocities and V_i is instantaneous velocity and u_i is unresolved velocity

$$\frac{\partial U_i}{\partial t} + U_j \frac{\partial U_i}{\partial x_j} + \frac{\partial \tau(V_i, V_j)}{\partial x_j} = -\frac{\partial p}{\rho \partial x_i} + \nu \frac{\partial^2 U_i}{\partial x_j \partial x_j}. \quad (2.6)$$

This above equation is Partially-averaged Navier-Stokes(PANS) equation. Where P is resolved pressure. the only term in above equation which is unresolved is $\tau(V_i, V_i)$, thus closing this term using Boussinessq relation. Now the equation as reads

$$\tau(V_i, V_j) = -2\nu_u S_{ij} + \frac{2}{3}k_u \delta_{ij} \quad (2.7)$$

where k_u is unresolved turbulent kinetic energy and The unresolved eddy viscosity is

$$\nu_u = C_\mu \frac{K_u^2}{\varepsilon_u} \quad (2.8)$$

S_{ij} is resolved stress tensor, reads

$$S_{ij} = \frac{1}{2} \left(\frac{\partial U_i}{\partial x_j} + \frac{\partial U_j}{\partial x_i} \right). \quad (2.9)$$

So this follows the same procedure as RANS, instead of averaging the whole spectrum of fluctuations, PANS is averaging only the unresolved turbulent variable and this has to be closed. The model equation for K_u and ε_u can be obtained from the RANS equation. Initially the PANS model is just 2 equation model based on $k - \varepsilon$. But recent research says that accuracy of PANS can be improved by adding two more equations velocity scale ratio and elliptical relaxation function f_u . Thus PANS becomes as four equation model $k - \varepsilon - \zeta - f_u$.

$$\begin{aligned} \frac{Dk_u}{Dt} &= P_u - \varepsilon_u + \frac{\partial}{\partial x_j} \left[\left(\nu + \frac{\nu_u}{\sigma_{k_u}} \right) \frac{\partial k_u}{\partial x_j} \right] \\ \frac{D\varepsilon_u}{Dt} &= C_{\varepsilon 1} P_u \frac{\varepsilon_u}{k_u} - C_{\varepsilon 2}^* \frac{\varepsilon_u^2}{k_u} + \frac{\partial}{\partial x_j} \left[\left(\nu + \frac{\nu_u}{\sigma_{\varepsilon u}} \right) \frac{\partial \varepsilon_u}{\partial x_j} \right] \\ \frac{D\zeta_u}{Dt} &= f_u - P_u \frac{\zeta_u}{k_u} + \frac{\zeta_u}{k_u} \varepsilon_u (1 - f_k) + \frac{\partial}{\partial x_j} \left[\left(\nu + \frac{\nu_u}{\sigma_{\zeta u}} \right) \frac{\partial \zeta_u}{\partial x_j} \right] \end{aligned} \quad (2.10)$$

$$L_u^2 \nabla^2 f_u - f_u = \frac{1}{T_u} \left(C_1 + C_2 \frac{P_u}{\varepsilon_u} \right) \left(\zeta_u - \frac{2}{3} \right)$$

where k_u is the turbulent kinetic energy, ε_u is the dissipation, σ_u is the turbulent Prandtl number, f_u is the relaxation function mentioned above, ν_u is the eddy viscosity, P the production term, L and T the length and time scales respectively.

$$f_k = \frac{k_u}{k} \quad ; \quad f_\varepsilon = \frac{\varepsilon_u}{\varepsilon}. \quad (2.11)$$

$$f_k = \frac{1}{\sqrt{C_\mu}} \left(\frac{\Delta}{\Lambda} \right)^{\frac{2}{3}} \quad ; \quad \Lambda = \frac{k^{\frac{3}{2}}}{\varepsilon} \quad ; \quad \Delta = (\Delta_x \Delta_y \Delta_z)^{\frac{1}{3}}. \quad (2.12)$$

Here, Λ is the integral length scale of turbulence and Δ is the grid cell dimension [9].

3 Model Description

The geometry, boundary conditions and numerical set-up are discussed in this section.

3.1 Geometry

The actual truck model have complex geometries which have simplified based on assumptions. Red line in figure 3.2 represents the geometry used for simulation. This is further simplified by smooth rounded corners at the sides of the truck. Side mirrors are assumed to have same height as the height of the truck, based on the previous research of guglie [1]. The computational domain was selected and all the dimensions are scaled with respect to the width of the truck body ($W = 0.4$ m), AFC was placed at a angle of 45 deg figure 3.7. The side mirror curves are provided by the truck company and the values are imported into Icem CFD.

Flow having velocity of 19.2 m/s was entering into the computational domain, which has Reynolds number of $5 * 10^5$.

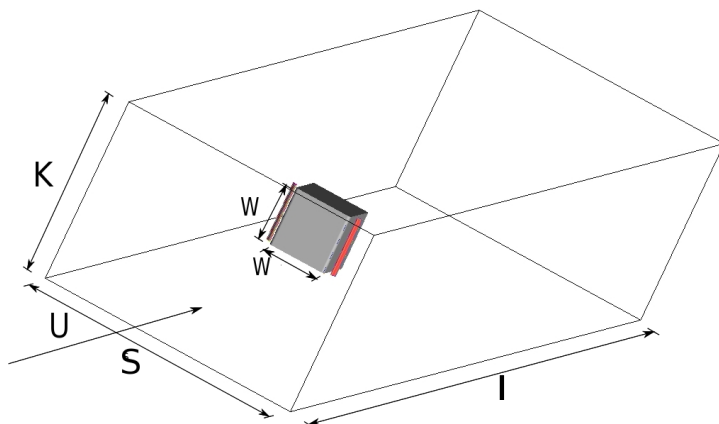


Figure 3.1: *Computational domain*



Figure 3.2: Geometrical assumption

Table 3.1: Computational domain measurements

Dimensions	[m]
W	0.4
I	17.5
K	3
S	4.5
R	0.05

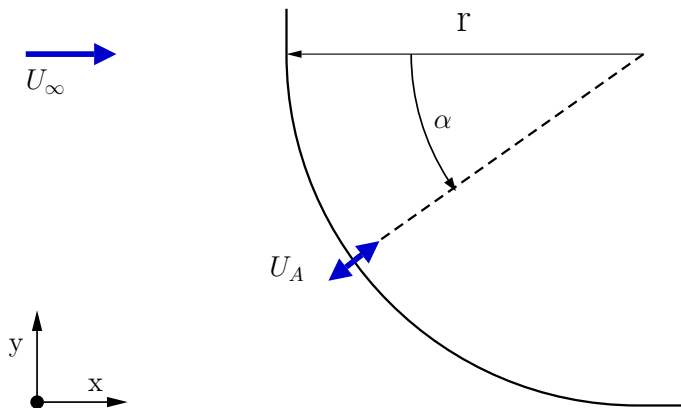


Figure 3.3: Top view of the A-pillar

3.2 Blocking and Meshing

3.2.1 Blocking

Commercial software ICEM CFD was used for blocking and hexa mesh generation. The advantage of hexa blocking was to create high quality hexaedral cell meshes. Initially the whole geometry was split into small block like structures using blocking tool in ICEM CFD. O-grid tool helps to concentrate cells around the different surface or parts [10] i.e. wall or boundary layer regions are fine meshed. Domain figure 3.7 has three O-grids and three C-grid, which helps us to create wall boundary layer around the truck body and mirrors figure 3.6.

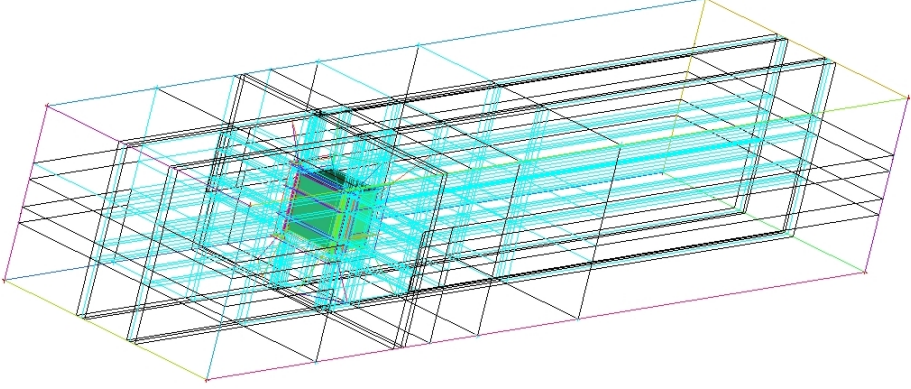


Figure 3.4: *Blocking of Computational domain in ICEM CFD*

3.2.2 Meshing

The blocks are filled with the hexa cells, by entering the number of nodes on each edges and cell distribution values was prescribed. These values are selected based on the Reynolds number value. Reynolds number and size are inversely proportional to each other. The cells should be concentrated in the region having small length scale, especially regions closer to the walls. The cell size calculation as follows

First step was to calculate the Reynolds number by using the free stream inlet flow velocity.

$$Re = \frac{2WU_{\infty}}{\nu} \quad (3.1)$$

Second step was to calculate skin friction coefficient [11] from Eq. 3.2

$$C_f = [2 \log_{10}(Re) - 0.65]^{-2.3} \quad \text{for } Re < 10^9 \quad (3.2)$$

Using skin friction coefficient, wall shear stress was computed.

$$\tau_w = 0.5\rho U_{\infty}^2 C_f \quad (3.3)$$

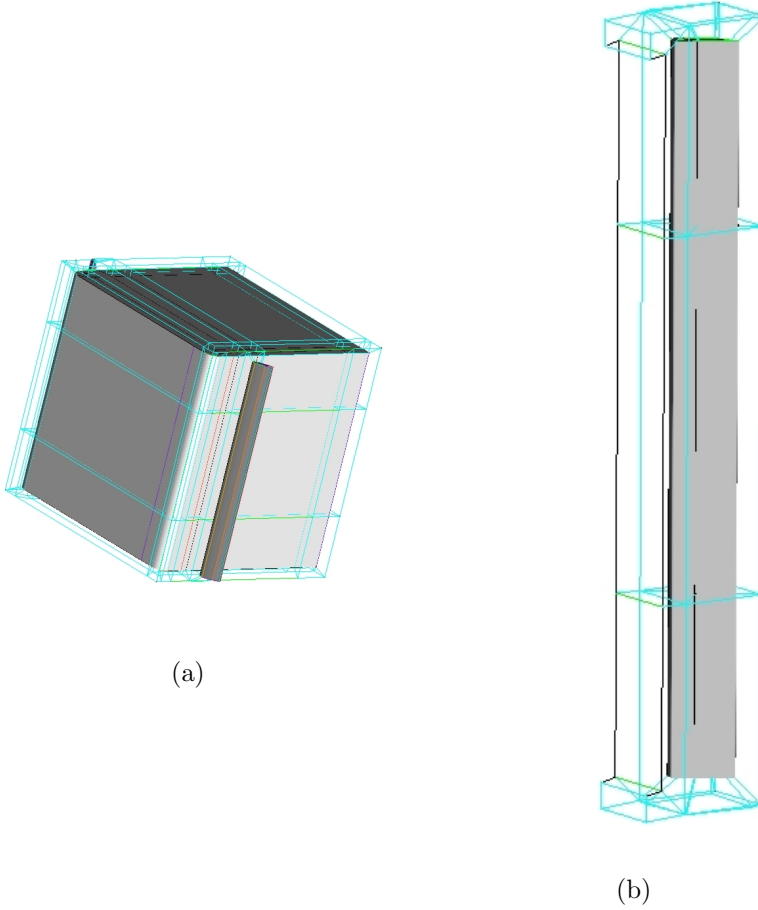


Figure 3.5: *O grid Blocking (a) O-Grid blocking of cube (b) O-Grid blocking of mirror*

Then the friction velocity u^* was computed using Eq. 3.4 y .

$$u^* = \sqrt{\frac{\tau_w}{\rho}} \quad (3.4)$$

At last u^* was then inserted in Eq. 3.5 to compute wall thickness of the first cell,

$$y = \frac{2\nu y^+}{u^*} \quad (3.5)$$

This above method was used to calculate the cell size for the wall region. the mesh

resolution for the stream and span-wise direction has to be calculated according to the turbulence model.

Mesh resolution for LES [1] Stream-wise (x^+) and Span-wise direction (z^+)

$$\Delta_x^+ < 100 \text{ and } \Delta_z^+ < 30$$

Mesh resolution for RANS

$$\Delta_x^+ < 400 \text{ and } \Delta_z^+ < 100$$

So, for PANS the resolution should be inbetween these values, hence the value selected[12]

$$\Delta_x^+ \approx 200 \text{ and } \Delta_z^+ \approx 60$$

$$\Delta_x^+ = \frac{\Delta_x u^*}{\nu} \quad \text{and} \quad \Delta_z^+ = \frac{\Delta_z u^*}{\nu} \quad (3.6)$$

The mesh quality in skewness and orthogonal quality was above 0.5. Mesh info

Number of cells (millions)	6.7
Time-Step (s)	0.00002
Free stream velocity (m/s)	19.2
Max y^+	2
mean y^+	0.2

3.3 Numerical set-up

This was the final stage of pre-processing were the boundary conditions, numerical shemes, turbulence model, timestep are entered to the commertial software AVL FIRE.

The flow was set to viscous and incompressible, 3-D unsteady flow. with air as a working fluid, density remains constant. Boundary conditions are given below

The turbulence model equation i.e. PANS was solved by the finite volume method. Second order accuracy schemes are selected to get accuracy in results. The simulations are carried out in AVL Fire software. [13]

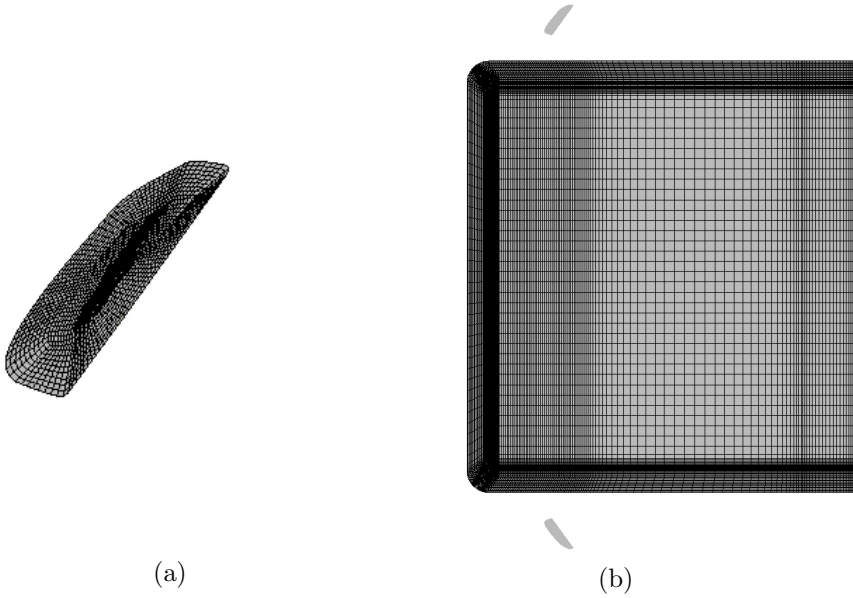


Figure 3.6: *Surface mesh of (a) Mirror (b) truck body*

Name	boundary condition
Inlet	Uniform velocity profile
Outlet	Homogeneous Neumann
AFC	Time varying velocity
Sides	Symmetry
Top and ground	Symmetry
Mirror and truck body	wall with no-slip

3.4 Post-processing

Details on two of the methods used to evaluate the results of the CFD simulations are given below. The post-processing of the results was carried out using ENSIGHT and MATLAB.

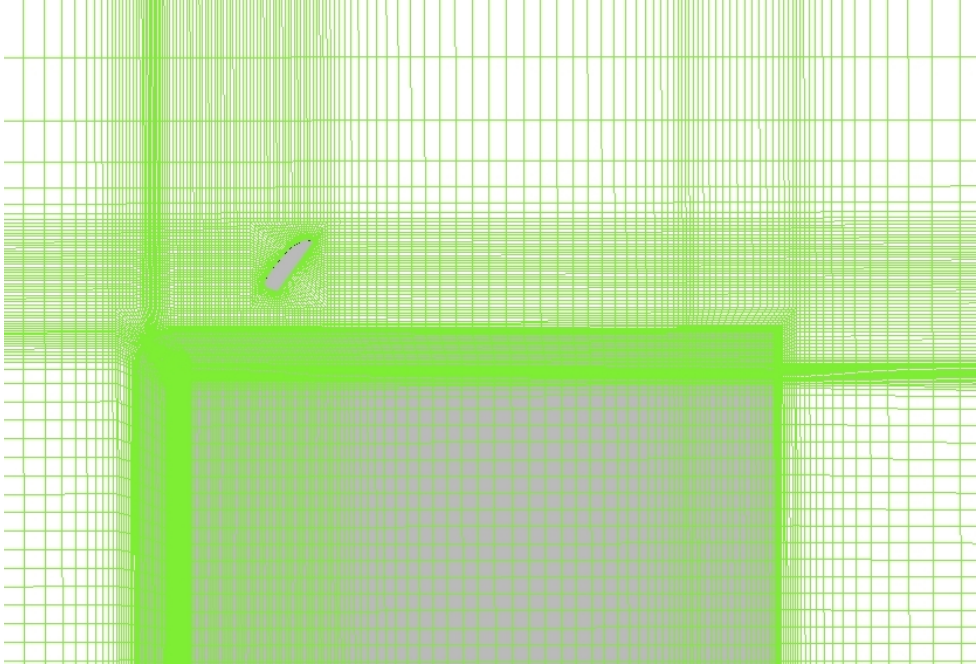


Figure 3.7: *O-grid mesh cut view around body and mirror*

4 Results and discussion

4.1 Un-actuated flow

Simulations were carried out for the Un-actuated flow to verify the time-step and mesh quality which were suitable to carry the simulation. This should be investigated by the values of CFL and y^+ . The CFL number and y^+ should be less than 1, from this figure 4.2 and 4.1 which gives the value of CFL number and y^+ number, in most of the parts the values fairly seem less than one. The mean y^+ number is 0.2 and highest value is 1.64. For CFL number the highest value is 2.6 at the corner of rounded edge that was due to the high velocity flow around the edges and the average velocity at the edges is around 35m/s.

For the PANS turbulence model, f_k value plays the major role which is the ratio of unresolved to total kinetic energy. From figure 4.4 the regions around the flow

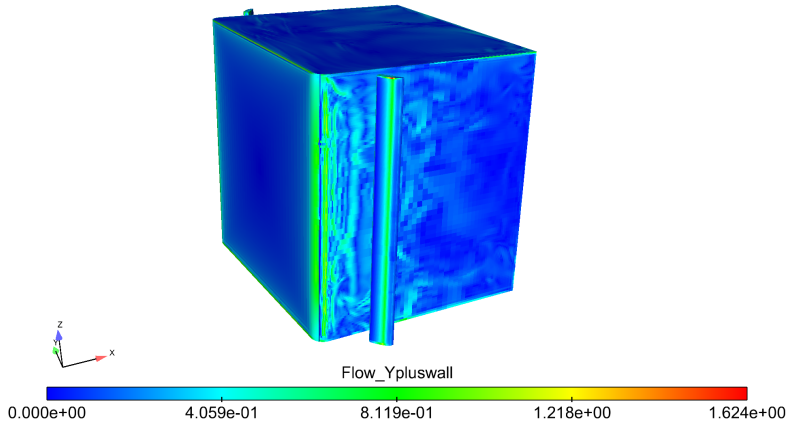


Figure 4.1: Y_{plus} value

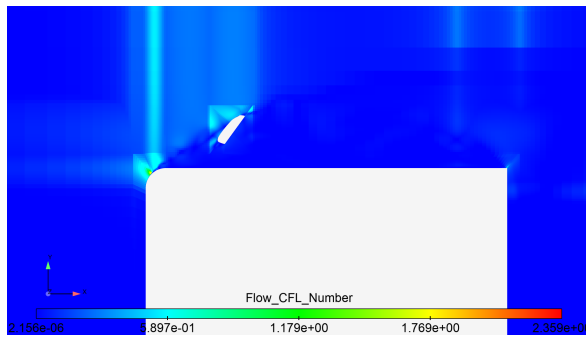


Figure 4.2: CFL Number for unactuated flow

separation are resolved since the f_k value is 0. After this the simulation for the Actuated can be carried, since the mesh, Time-step and PANS model seems to work well.

The averaged flow velocities are calculated once the flow becomes fully developed, this can be identified once the flow starts to fluctuate around the same value. From figure 4.3 this shows after the flow time reaches 0.4 sec the flows starts to become fully developed. But in order to make sure the flow is fully developed the averaging is done after 2 flow passages (1 flow passage can be defined as time taken by the single fluid particle to travel entire computational domain in stream-wise direction), and the averaging is done for 3 flow passages.

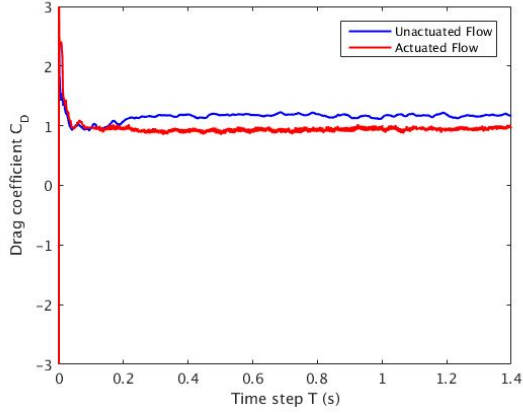


Figure 4.3: *Coefficient of drag*

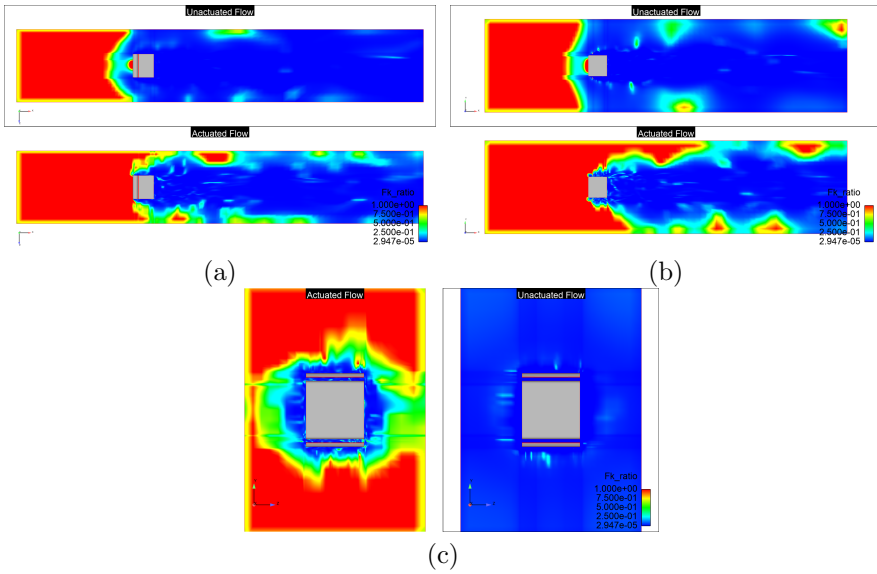


Figure 4.4: f_k value with respect to 3 planes with Actuated flow (below) and Unactuated Flow (above) (a) Y-plane at mid of computational domain (b) Z-plane at mid of computational domain (c) X-plane at 0.01 m

4.2 comparison between controlled and uncontrolled flow

For the actuated flow, The ZNMF actuator is used which has periodic cycle of suction and blowing. This can be introduced to the simulation by time varying boundary condition to the thin AFC surface in geometry. The formula used for periodic suction and blowing as follows

$$\mathbf{U}_{AFC} = -U_A \sin(2\pi f_A t) \quad (4.1)$$

U_A is the actuation velocity which is 5 m/s and Frequency (f_A) of 144 Hz selected from guglielmo work. This formula 4.1 is implemented in the boundary condition of AFC in FIRE 2014.

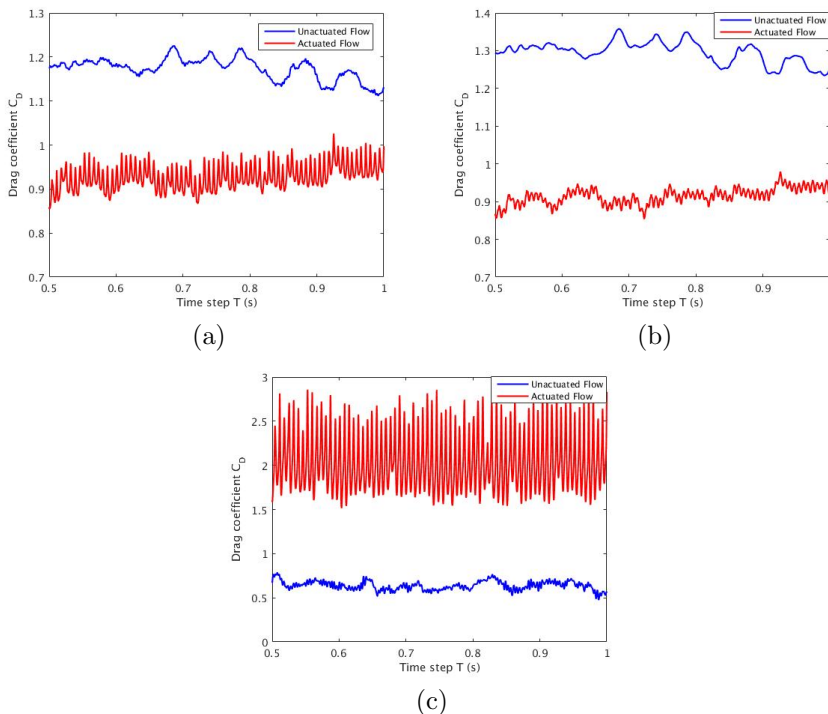


Figure 4.5: *Coefficient of Drag (a) Overall drag coefficient (b)Truck cabin drag coefficient (c) Mirror drag coefficient*

The ultimate aim of actuators which are used at a-pillar of truck is to reduce

the aerodynamic drag of the truck. The non-dimensional number called co-efficient of drag is calculated to study about the aerodynamic drag for the actuated and un-actuated flow, From figure 4.5 (a) The overall drag co efficient for Un-actuated and Actuated is 1.18 and 0.88 respectively. So the overall reduction in drag is about 25 percent. from the guglielmo work the overall drag reduction for the same set-up is about 31 percent. this suggest that side mirrors are influencing increase in drag. The coefficient of drag separately for truck cabin and mirrors are calculated and this can be seen in figure 4.5 interesting observation found for the mirror drag co-efficient, were there is increase in co-efficient of of drag due to actuated flow. The reasons for increase in drag co-efficient is discussed later by post-processing the various field variables.

From figure 4.6, reasons for drag increase in side mirrors is elaborated . In general drag can be caused by two different forces pressure and friction force. For the actuated flow the pressure on the front side of the side mirror is high when compared with the un-actuated flow, thereby causing the increase in coefficient of drag C_d . For the un-actuated flow the pressure force is comparatively less so the majority of the drag is due to the frictional force and frictional force is low. The side mirrors are placed in that position to avoid the pressure drag for the un-actuated flow.

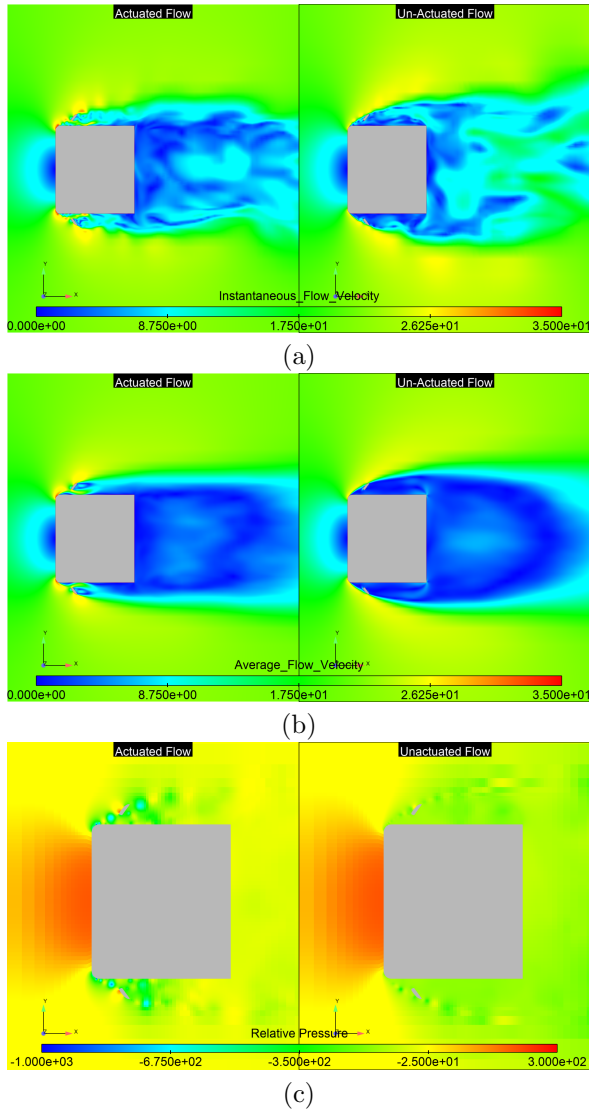
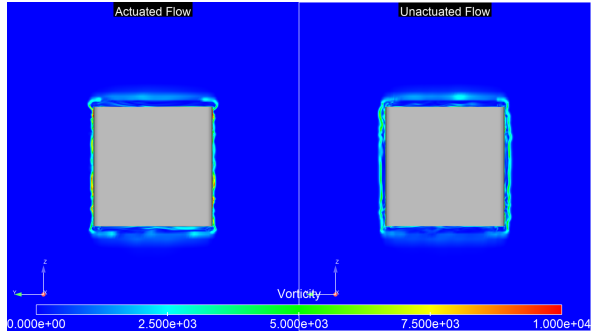
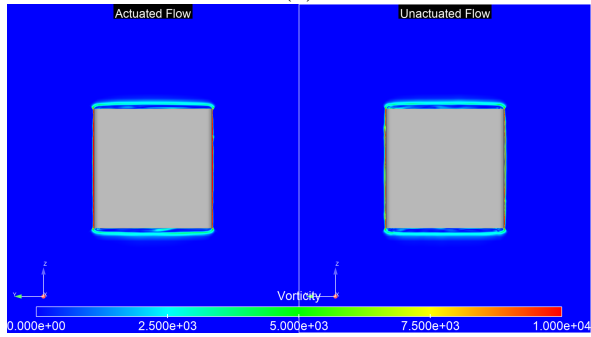


Figure 4.6: Actuated flow on left and Un-actuated Flow on right (a) Instantaneous velocity flow (b) Average Flow velocity (c) Relative pressure plot

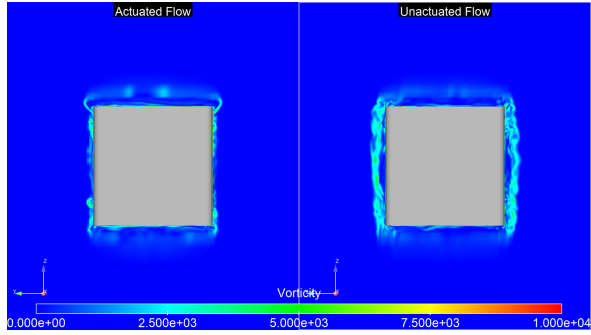
From figure 4.7 and 4.8 which shows the vorticity plot. This shows how the flow energy is dissipated into the streamline flow due to Cascade process by transferring energy from one eddies to other.eddies basically carry the energy and for the un-



(a)



(b)



(a)

Figure 4.7: *Flow vorticity with respect to X-plane of computational domain with Actuated flow on left and Un-actuated Flow on right (a) X-Plane at 0.03m (b) X-Plane at 0.02m (c) X- plane at 0.05m*

actuated flow the flow is not attached to the body of the truck, but for the actuated flow the flow tends to attach on the body of the truck.

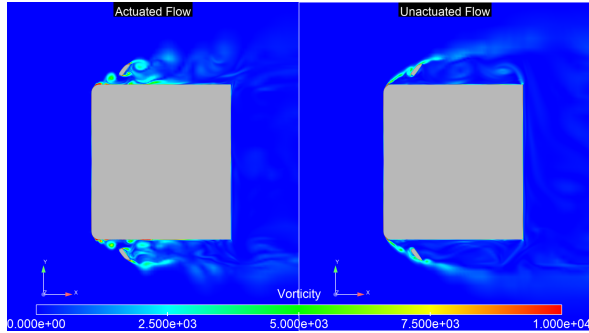


Figure 4.8: *Flow vorticity with respect to Z-plane of computational domain with Actuated flow on left and Un-actuated Flow on right Z-Plane at midrange*

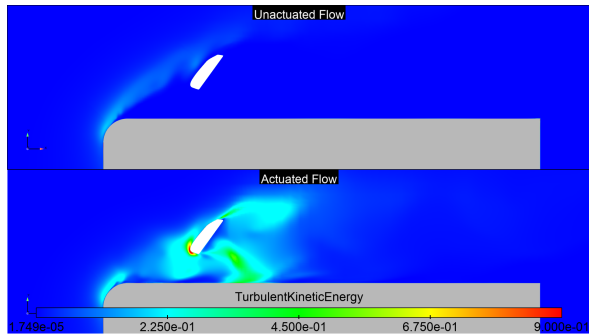
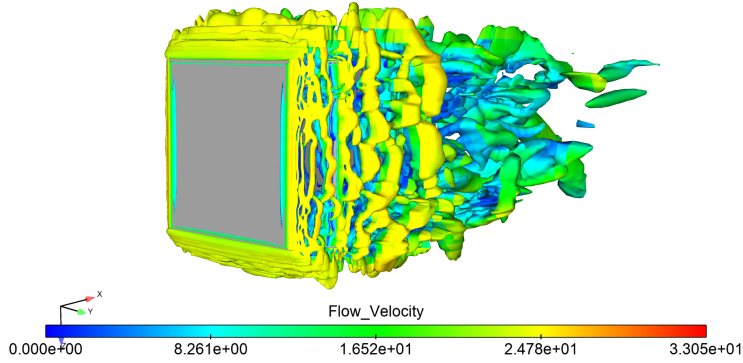
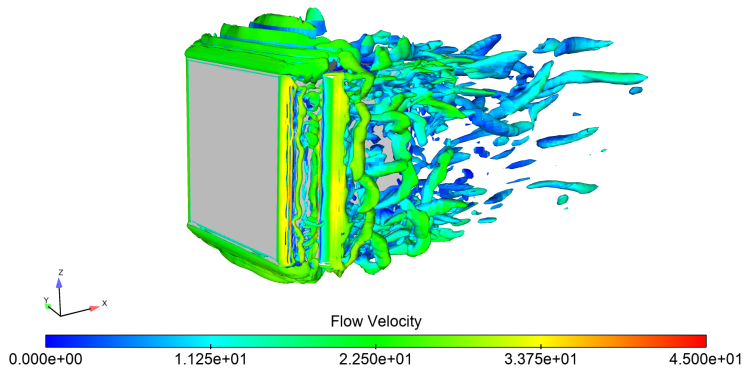


Figure 4.9: *Turbulent kinetic energy plot for Unactuated flow (above) and Actuated flow (below)*

Interesting observation is noted in turbulent kinetic energy 4.9, for the unactuated flow the turbulent turbulent kinetic energy is less than actuated flow. in study it shows separation region size is directly proportional to the turbulent kinetic energy region. since there are side mirrors, they create velocity fluctuations which increases turbulent kinetic energy . In simple the energy is extracted from the mirrors and this is the reason for increased drag force on the mirrors.



(a)



(b)

Figure 4.10: *The iso-surface of the instantaneous second invariant of the velocity gradient $Q=10000$ (a) For Un-actuated flow (b) For Actuated flow*

5 Conclusions and future work

The overall objective of the project work is to investigate the effects of side mirrors has when the flow is actuated. The overall drag reduction of 25 percent is achieved. From the conclusion point there is reduction in drag, but due to actuation the pressure force on side mirrors increases. This pressure force creates fluctuating vorticity at the side mirrors which makes side mirrors to experience high stress.

For the future work, since there has been rapid development in technology. There is more possibility that side mirrors could be replaced by cameras. For the AFC

actuated flow the removal of side mirror can cause further drag reduction from 25 percent to 31 percent. So the future should go ahead in plan for removing side mirrors.

References

- [1] L. H. V. C. B. B. Guglielmo minelli Erwin Adi Hartono and S. Krajnovic. PANS validation and active flow control for a generic truck cabin using synthetic jets: a numerical and experimental study. *International Journal of Heat and Fluid Flow* **37** (2017), 109–122.
- [2] Y. A. Cengel and J. M. Cimbala. *Fluid mechanics: fundamentals and applications*. International edition. New York, United States of America: McGraw-Hill, 2006.
- [3] C. Louis N. and M. Sheplak. Actuators for active flow control. *Annu Rev.FluidMech* **43.1** (2011), 247–272.
- [4] G. D. Raithby and E. R. G. Eckert. The Effect of Support Position and Turbulence Intensity on the Flow Near the Surface of a Sphere. *Wärme- und Stoffübertragung* **1** (2 1968).
- [5] E. Guilmineau, O. Chikhaoui, G. Deng, and M. Visonneau. Cross wind effects on a simplified car model by a DES approach. *Computers and Fluids* **78** (2013), 29–40.
- [6] M. L. Shur, P. R. Spalart, M. K. Strelets, and A. K. Travin. A hybrid RANS-LES approach with delayed-DES and wall-modelled LES capabilities. *International Journal of Heat and Fluid Flow* **29** (2008), 1638–1649.
- [7] B. Basara, S. Krajnović, and Z. Pavlovic. Near-Wall Formulation of the Partially Averaged Navier-Stokes Turbulence Model. *AIAA Journal* **49.12** (2011), 2627–2636.
- [8] S. Krajnović and G. Minelli. “Status of PANS for Bluff Body Aerodynamics of Engineering Relevance”. *Progress in Hybrid RANS-LES Modelling*. Cham, Switzerland: Springer International Publishing, 2015, 399–410.
- [9] S. Krajnović, R. Lárusson, and B. Basara. Superiority of PANS compared to LES in predicting a rudimentary landing gear flow with affordable meshes. *International Journal of Heat and Fluid Flow* **37** (2012), 109–122.
- [10] *ANSYS ICEM CFD User’s Manual*. ANSYS inc. Canonsburg, United States of America, 2013. URL: <http://148.204.81.206/Ansys/150/ANSYS%20ICEM%20CFD%20Users%20Manual.pdf>.

- [11] H. Schlichting. *Boundary-layer theory*. 7th ed. New York, United States of America: McGraw-Hill, 1979.
- [12] G. Minelli. Department of Applied Mechanics, Chalmers University of Technology. Private communication. Göteborg, Sweden, 2015.
- [13] *AVL Fire manual*. AVL 2014. Graz, Austria, 2014.